

Collision Risk Estimation via Loss Prediction in End-to-End Autonomous Driving

Ziliang Xiong^{1*}, Shipeng Liu¹, Nathaniel Helgesen¹, Hongwei Li³,
Joakim Johnander^{1,2}, Per-Erik Forssén¹

¹Department of Electrical Engineering, Linköping University, Linköping, 58183, Sweden.

²Zenseact, Lindholmspiren 2, Gothenburg, 41756, Sweden.

³Department of Biomedical Engineering and Department of Diagnostic Radiology,
National University of Singapore, 21 Lower Kent Ridge Road, 119077, Singapore.

*Corresponding author(s). E-mail(s): ziliang.xiong@liu.se;

Contributing authors: shipeng.liu@liu.se; nathaniel.helgesen@liu.se;
hongwei.bran.li@nus.edu.sg; joakim.johnander@zenseact.com; per-erik.forssen@liu.se;

Abstract

Collision risk estimation and avoidance play central roles in the safety of autonomous driving (AD) systems. Recently emerged end-to-end AD systems gain collision avoidance ability by minimizing losses to penalize planning trajectories that are too close to other objects. Despite a significant collision rate during testing, most end-to-end planners do not explicitly quantify the collision risk in their outputs. To address this, we introduce RiskMonitor, an efficient plug-and-play module that interprets planning and motion tokens from state-of-the-art end-to-end planners to estimate collision risk. Inspired by loss prediction based uncertainty quantification, RiskMonitor predicts whether the collision loss—commonly adopted to train end-to-end planners—is positive along planned waypoints, framing collision risk estimation as a binary classification task. We evaluate RiskMonitor on the real-world nuScenes dataset (open-loop) and the neural-rendering based simulator, NeuroNCAP (closed-loop). Our token-driven method outperforms prediction-driven approaches, including deterministic rules, Gaussian mixture models, and Monte Carlo Dropout. When integrated with a simple braking policy, RiskMonitor improves collision avoidance ability by **66.5%** in a closed-loop test on safety-critical scenarios. These results demonstrate that monitoring collision risk using plan and motion tokens enhances the safety of end-to-end AD without retraining it.

Keywords: Autonomous driving, Collision risk, Motion planning, Uncertainty quantification

1 Introduction

For safety reasons, collision checking and avoidance are necessary parts of the perception and planning system for autonomous driving. Recently, several works (Hu et al. 2023; Jiang et al. 2023; Zheng et al. 2024; Chen et al. 2024) have

proposed end-to-end planners which map sensor input to planned trajectories for the ego-vehicle to follow. In these works, collision avoidance is learned during the planning stage by optimizing a collision constraint alongside a large set of other loss terms. This collision constraint penalizes planned trajectories that are too close to the

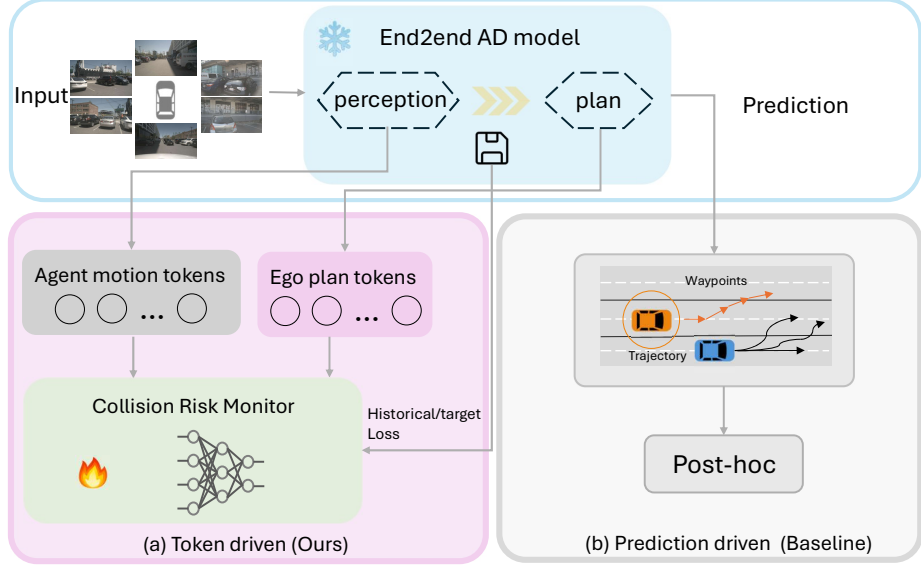


Fig. 1: Two approaches for monitoring the collision risk in frozen end-to-end planners. (a). Our proposed token-driven: Train RiskMonitor to decode road user motion tokens and ego planning tokens from E2e planners; (b). Prediction-driven: The monitor could be post-hoc, such as a rule, GMM, or MC Dropout, but these suffer from accumulated prediction error.

trajectories of other objects (Hu et al. 2023; Jiang et al. 2023). However, due to the limited number of safety-critical behaviors in the training data, these methods suffer from a significant collision rate during both open-loop and closed-loop testing. One way to improve the collision avoidance performance is to train end-to-end planners on more safety-critical data. This is time-consuming and expensive in the real world; thus, research such as (Ljungbergh et al. 2024; Jia et al. 2024) proposes collecting data via simulation. However, this introduces the risk of a domain shift between the simulated and real-world data, thus hampering the generalization. Here, we instead monitor the collision risk during inference time, which requires no retraining of end-to-end planners.

Koopman and Wagner (2016) proposed the decomposition of a monitor and actuator architecture to enhance AD safety level. The actuator performs the primary functions, and the monitor conducts an acceptance test or other forms of behavioral validation. End-to-end planners do not explicitly monitor their behavior in this way, e.g., they do not estimate the collision risk of the planned trajectory while driving. Aligned with Koopman’s decomposition philosophy, we propose

integrating a monitor module into the end-to-end planner to explicitly estimate the collision risk of the planned trajectory. A straightforward approach (See Fig. 1 (b)) to such a monitor is to leverage physically interpretable predictions from end-to-end planners, specifically by comparing the planned trajectory for the ego-vehicle with the predicted trajectories of other road users. This comparison can employ deterministic rules, such as whether intersection over union (IoU) exceeds a threshold, or probabilistic rules, such as the likelihood under a Gaussian mixture model (GMM) (Hu et al. 2018). However, our experimental results indicate that prediction errors in end-to-end planners render this approach unreliable.

Instead, we propose implementing the monitor module using loss prediction. *Loss prediction* (Yoo and Kweon 2019; Kirchhof et al. 2023) is a post-hoc uncertainty quantification method that uses an auxiliary network to map deep features to estimated loss values, providing an error estimate for predictions. Compared to previous loss prediction work, end-to-end planners are more complex models, supervised by a large number of loss functions, but only one of them (the collision constraint) is

of interest. The question we try to answer in this work is *whether collision risk can be estimated through loss prediction*.

As end-to-end planners are typically partially supervised by a collision loss during training, the collision risk monitor could be a small neural network that maps the end-to-end planner’s tokens to an estimate of the collision loss value, which can then be interpreted as the collision risk. Thus, we introduce a novel and efficient monitor module, RiskMonitor, which predicts the collision risk for the end-to-end plan outcome. As Fig. 1 (a) indicates, our RiskMonitor is trained with motion and planning tokens from a given frozen end-to-end planner as inputs and historical collision loss values as targets. RiskMonitor prediction can be used during inference as a binary collision prediction. Compared to modular AD systems, a significant advantage is that end-to-end planners avoid information loss caused by engineered interfaces between modules and by handcrafted rules. Our proposed token-driven approach enables the monitor to share such an advantage.

We evaluate RiskMonitor in both real-world *open-loop* and neural-rendering based *closed-loop* benchmarks. As an open-loop benchmark, we use nuScenes (Caesar et al. 2020), which contains real-world driving video sequences. As a closed-loop benchmark, we use NeuroNCAP (Ljungbergh et al. 2024), which contains realistic safety-critical scenarios with sensor input created by neural rendering. Through extensive evaluation, we show that RiskMonitor outperforms the deterministic rule, GMM, and Monte Carlo Dropout (Gal and Ghahramani 2016). We further validated the actual collision-avoidance performance of RiskMonitor in NeuroNCAP by harshly braking if the predicted collision risk is high. Our results show that this simple strategy reduces the collision rate on NeuroNCAP by 67%.

To summarize, our main **contributions** are:

1. We introduce collision risk estimation (CRE) for planned trajectories as a side task for end-to-end AD to enhance safety, and propose a plug-and-play module, RiskMonitor, to solve it.
2. We show that loss prediction is applicable to end-to-end AD models, which are substantially more complex than models previously tested

in loss prediction. We also show that loss prediction can be treated as binary classification rather than regression.

3. In an extensive evaluation across end-to-end planners, our RiskMonitor module manages to capture 50% of all collisions with 45.6% precision on nuScenes and with 67.5% precision on NeuroNCAP. Moreover, RiskMonitor reduces the collision rate on NeuroNCAP by 66.5% on average.

2 Related Work

End-to-End Autonomous Driving: Hu et al. (2023) aim to secure the advantages of both a modular stack and an end-to-end planner. To this end, they propose a modular method, UniAD, comprising a bird-eye view (BEV) encoder (Li et al. 2022), a combined detector and tracker (Meinhardt et al. 2022), a map encoder, a motion forecaster, an occupancy grid estimation module, and a planner, where the information flow between different modules is learned end-to-end. A few works follow a similar design philosophy. VAD (Jiang et al. 2023) is more computationally efficient because it utilizes a vectorized representation. PPAD (Chen et al. 2024) iteratively couples prediction and planning to enable adaptive, interaction-aware planning. Zheng et al. (2024) employ a gated recurrent unit to progressively predict the next future in the latent space and use a decoder to obtain explicit trajectories. These works have in common that the planning heads are all explicitly supervised by a collision loss term that punishes the planned trajectory for overlapping with obstacles. We chose UniAD, VAD for the experiments. UniAD and VAD are shown to work in conjunction with NeuroNCAP, a realistic simulator we leverage to explore how RiskMonitor performs on safety-critical scenarios.

Closed-loop Evaluation: End-to-end planning has been analysed both in the CARLA (Dosovitskiy et al. 2017) closed-loop simulator (Chen et al. 2021; Codevilla et al. 2018; Prakash et al. 2021; Wu et al. 2023) and on real data (Hu et al. 2021; Khurana et al. 2022; Hu et al. 2022). In NeuroNCAP (Ljungbergh et al. 2024), an end-to-end planner receives sensor input and outputs the planned trajectory. The planned trajectory is then passed to a controller and vehicle kinematics model that

moves the ego vehicle forward. Finally, the NeRF-based renderer NeuRAD (Tonderski et al. 2024) creates sensor data for the next frame of the 3D scene. In this way, end-to-end AD models can be evaluated in a closed-loop manner. NeuroNCAP generates three types of safety-critical scenarios, namely “stationary”, “side”, and “frontal”. We adopt NeuroNCAP rather than CARLA since it concentrates on safety-critical scenarios.

Uncertainty Quantification: Trajectory forecasting methods typically model future object states probabilistically (Hu et al. 2021; Akan and Güney 2022; Deo et al. 2022). Neumeier et al. (2024) boost the generation of physically feasible trajectories by incorporating guidance from a UQ module, yet the UQ performance is not explicitly evaluated. In out-of-distribution (OOD) scenarios (Malinin et al. 2021; Bahari et al. 2021), performance degradation and lack of predictive uncertainty can lead to severe consequences. Wiederer et al. (2023) use an encoder-decoder-like model to predict trajectory and then jointly estimate OOD score and in-distribution (ID) uncertainty score. They treat ID uncertainty as a LP regression task (Yu et al. 2024; Yoo and Kweon 2019), training a small MLP to predict future trajectory error. Though similar, we instead frame loss prediction as a classification task, which improves interpretability and enables integration with more complex end-to-end planners. In end-to-end planners (Hu et al. 2023; Jiang et al. 2023), the future trajectory of a road user is modeled as an ensemble of possible candidates along with probabilities. The uncertainty in these methods quantifies the ambiguity of the trajectory and not the collision risk. Cai et al. (2020) introduce a probabilistic motion planning network which outputs a distribution of future motion based on the Gaussian mixture model, but without explicit collision risk awareness. Concurrent work, Redoubt (Wang et al. 2025), proposes to predict the collision risk of object-level planners, assuming the availability of ground-truth objects and lanes. In contrast, our work focuses on end-to-end planning and presents results in safety-critical scenarios.

Collision Risk Modelling and Avoidance: For safe planning in AD, one must quantify the collision risk associated with the planned trajectory. There are two main approaches to probabilistic CRE: collision state probability (CSP)

and collision event probability (CEP) (Philipp and Goehring 2019). CSP estimates the probability density that two objects spatially overlap at a specific future time. Houenou et al. (2014); Lambert et al. (2009); Toit and Burdick (2011) use Monte Carlo to calculate CSP but suffer from high sample complexity and latency. CEP extends this by estimating the probability density that a collision occurs at any point over a future time horizon (Altendorfer and Wilkemann 2017; Nordlund and Gustafsson 2008). Philipp and Goehring (2019) use the geometric simplification of a collision octagon to enable efficient closed-form approximations under Gaussian uncertainty. However, all the rule-based CRE oversimplify the driving scenarios and are not evaluated on large datasets. As risk modeling is a context-dependent task, it has been integrated into collision-avoidance planning (Huang et al. 2021; Yang et al. 2024) in the field of model predictive control (MPC). We argue that such risk modelling is essential for the interpretability and safety of end-to-end planners.

3 Preliminaries

Sec. 3.1 first gives the task formulation of collision risk estimation. Afterwards, Sec. 3.2 reviews the theory of loss prediction.

3.1 Task Formulation

Modern end-to-end planners typically predict trajectories over a short fixed time horizon. Unlike previous methods that calculate CEP density as a time-evolving process (Philipp and Goehring 2019), we aim to directly predict the event-level collision probability over the entire horizon, i.e., the probability that a collision occurs at any time within the horizon. More specifically, the planning outcome is a unimodal trajectory¹ consisting of waypoints, $\hat{\tau}_{\text{plan}} \in \mathbb{R}^{N_T \times 2}$, where N_T is the number of predicted future waypoints in the time horizon T and 2 corresponds to 2D coordinates in the ego-vehicle centered BEV frame.

The collision risk over the time horizon T is then formally expressed as

¹Though some planners predict a planning vocabulary, the controller requires a *unimodal*, or singular, trajectory.

$$\begin{aligned}
& P(\text{collision} \mid \hat{\tau}_{\text{plan}}) \\
&= \int_0^T p\left(\sum_i^{N_a} \text{IoU}(\hat{\tau}_{\text{plan}}(t), \tau_{\text{motion}}^i(t)) > 0\right) dt , \tag{1}
\end{aligned}$$

where the true future trajectory for the i th road user is $\tau_{\text{motion}}^i \in \mathbb{R}^{N_T \times 2}$ and the total number of road users is N_a . With a slight abuse of notations, both $\hat{\tau}_{\text{plan}}$ and τ_{motion}^i take the object geometry dimension into account during IoU calculation.

3.2 Loss Prediction

The core idea of loss prediction is to add an auxiliary module to a target model Θ_{target} (Yoo and Kweon 2019), for instance, a classifier, to predict its loss value as an indicator of prediction uncertainty. Given a training sample pair (\mathbf{x}, y) , we obtain a target prediction \hat{y} and intermediate features h_i through the target model as in Eq. (2).

$$\hat{y}, h_1, \dots, h_n = \Theta_{\text{target}}(\mathbf{x}) , \tag{2}$$

$$h = \{h_1, h_2, \dots, h_n\}, n \geq 1 , \tag{3}$$

$$L_{\text{target}} = \mathcal{L}_{\text{target}}(\hat{y}, y) . \tag{4}$$

The target loss value L_{target} can be computed with the annotation y as in Eq. (4). Meanwhile, an auxiliary module Θ_{loss} predicts the loss value of the target model with a set of features h as input,

$$\hat{L}_{\text{target}} = \Theta_{\text{loss}}(h) , \tag{5}$$

$$L_{\text{loss}} = \mathcal{L}_{\text{loss}}(\hat{L}_{\text{target}}, L_{\text{target}}) . \tag{6}$$

The target loss value L_{target} serves as the ground truth for the loss predictor Θ_{loss} . Formally, the total loss function used to train the target model Θ_{target} and the loss prediction module Θ_{loss} is

$$\mathcal{L}_{\text{target}}(\hat{y}, y) + \lambda \mathcal{L}_{\text{loss}}(\hat{L}_{\text{target}}, L_{\text{target}}) , \tag{7}$$

where λ is a predefined constant scaling factor. Previous loss prediction work typically trains the auxiliary module as a regressor using L_2 loss (Yoo and Kweon 2019) or a ranking-based objective (Kirchhof et al. 2024) to detach from the scale of target loss L_{target} .

To avoid Θ_{loss} from interfering with Θ_{target} during training, Kirchhof et al. (2024) proposed to pretrain Θ_{target} and then freeze it. To speed

up training, (h, L_{target}) pairs are cached during the training of Θ_{target} , and Θ_{loss} is then trained separately. After training, the loss prediction module Θ_{loss} becomes an uncertainty quantifier, with a higher predicted value indicating that the target model is more uncertain (Kirchhof et al. 2023). Next, we extend loss prediction to predict whether modern end-to-end planners will generate colliding plans.

4 Method

We adapt loss prediction to collision risk estimation (CRE) for end-to-end planners in Sec. 4.1. Sec. 4.2 introduces our RiskMonitor architecture. Finally, Sec. 4.3 introduces techniques for handling class imbalance in real-world data.

4.1 Collision risk estimation

For driving safety, we are particularly interested in predicting whether the planned trajectory will cause a collision. To train RiskMonitor, we first need to determine which loss value in the end-to-end AD model should be used as the training label \hat{L}_{target} and which features to include in the input set h .

Choice of target loss: Prior work on loss prediction (Yoo and Kweon 2019; Kirchhof et al. 2023) typically considers models supervised by a small number of loss terms; in contrast, state-of-the-art end-to-end planners are more complex and supervised by hundreds of loss terms. They comprise multiple modules designed to handle different tasks, e.g., motion prediction and planning (Hu et al. 2023; Jiang et al. 2023). There is no single loss as in standard loss prediction tasks; instead, different modules have distinct functions, and each can have multiple parts. This results in a large and heterogeneous set of loss components, raising the question of which loss should be selected as the prediction target.

For training RiskMonitor, we focus on the collision loss component present in the planning module. The planning module loss function has multiple parts, including an imitation loss $\mathcal{L}_{\text{imitation}}$ and a collision loss $\mathcal{L}_{\text{collision}}$. The imitation loss is usually the L_2 distance to the ground-truth trajectory so that the model learns to exhibit a human-like planning capability, while the collision loss penalizes plans that result in collisions

with other road users on the road. To apply loss prediction, we adopt the collision loss component from the last transformer layer, $\mathcal{L}_{\text{collision}}$, and train Θ_{loss} to predict its value.

Our RiskMonitor frames loss prediction as a binary classification task. The scale of $L_{\text{collision}}$ does not reflect the real-world accident severity of collisions, as it is the sum of IoU and does not account for speed. Consequently, treating CRE as a regression task—as is standard in prior loss prediction work (Yoo and Kweon 2019; Kirchhof et al. 2024)—is suboptimal in this setting. Instead, we note that whether the collision loss value is positive indicates if a collision is going to occur along the planned trajectory.² Thus, it is natural to treat CRE as a binary classification task instead and predict the probability of a collision occurring along the planned trajectory $\hat{\tau}_{\text{plan}}$,

$$P(\text{collision} \mid \hat{\tau}_{\text{plan}}) = \Theta_{\text{RiskMonitor}}(h) . \quad (8)$$

Then, RiskMonitor is trained using

$$L_{\text{loss}} = \mathcal{L}_{\text{RiskMonitor}}(P(\text{collision} \mid \hat{\tau}_{\text{plan}}), L_{\text{collision}}) , \quad (9)$$

where $\mathcal{L}_{\text{RiskMonitor}}$ is the cross-entropy loss or the focal loss if there is class imbalance (See Sec. 4.3). **Choice of features:** An open question is which features h should be fed into $\Theta_{\text{RiskMonitor}}$. Given a training sample \mathbf{x} , each module of the end-to-end planner produces separate predictions using many consecutive intermediate features. Normally, rule-based methods, e.g. in Sec. 5.1, make use of the motion prediction $\hat{\tau}_{\text{motion}}$ and the planned ego trajectory $\hat{\tau}_{\text{plan}}$ to predict CEP. We note that this motion prediction is intentionally stochastic (Hu et al. 2023; Jiang et al. 2023), as end-to-end AD models typically predict multimodal trajectories to balance the unpredictability of other drivers’ intentions. Since both $\hat{\tau}_{\text{plan}}$ and $\hat{\tau}_{\text{motion}}$ are outputs from individual transformer modules, we can also output the respective planning token h_{plan} and road user tokens h_{motion} . Because these tokens are the layers directly before $\hat{\tau}_{\text{plan}}$ and $\hat{\tau}_{\text{motion}}$, they conceivably contain more information, thus we opt to use them as inputs. Formally, the

outputs we cache from the end-to-end planner are

$$\hat{\tau}_{\text{plan}}, \hat{\tau}_{\text{motion}}, h_{\text{plan}}, h_{\text{motion}} = \Theta_{\text{planner}}(\mathbf{x}) . \quad (10)$$

4.2 RiskMonitor Architecture

To model the interaction between the planned trajectory and surrounding agents, we employ a transformer decoder architecture. The decoder takes the planning tokens $h_{\text{plan}} \in \mathbb{R}^d$ as input and attends to the set of agent-motion tokens $H_{\text{motion}} \in \mathbb{R}^{N_a \times d}$, where N_a is the number of road users. Specifically, original motion tokens are in the shape of $h_{\text{motion}} \in \mathbb{R}^{N_a \times N_m \times d}$, where N_m is the number of modalities. Motion tokens are passed through an MLP fuser to flatten out the second dimension.

The core operation is the multi-head cross-attention mechanism (Vaswani et al. 2017), which computes attention weights between the query and the key-value pairs derived from H_{motion} . For each head $i \in \{1, \dots, h\}$, we define

$$\text{head}_i = \text{softmax} \left(\frac{(QW_i^Q)(KW_i^K)^\top}{\sqrt{d_k}} \right) (VW_i^V) , \quad (11)$$

where $Q = h_{\text{plan}}$, $K = H_{\text{motion}}$, $V = H_{\text{motion}}$. The matrices W_i^Q, W_i^K, W_i^V are learned projections for the i -th head, and d_k is the dimension per head. The outputs of all heads are concatenated and projected to form the decoder output as

$$z = \text{Concat}[\text{head}_1, \dots, \text{head}_h]W^O , \quad (12)$$

where $W^O \in \mathbb{R}^{(h \cdot d_v) \times d}$ is the output projection matrix. Finally, the collision risk is predicted by passing z through a feed-forward network followed by a sigmoid activation as

$$\Theta_{\text{RiskMonitor}}(h) = \sigma(\text{MLP}(z)) . \quad (13)$$

This formulation allows the decoder to capture complex interactions between the planned trajectory and multiple agents across modalities through multi-head attention.

²See Eq. (4) in VAD (Jiang et al. 2023) for an example.

4.3 Handling Data Imbalance

Real-world AD datasets are typically imbalanced as samples without collisions greatly outnumber those with collisions. To alleviate this issue, we propose combining the bagging ensemble and undersampling (Westny et al. 2021) with the focal loss (Lin et al. 2017). Given the set of collision samples P and the set of noncollision class examples Q , $|P| < |Q|$. In bagging, Q is split into N subsets, Q_1, Q_2, \dots, Q_N , and each subset is combined with P to form N training sets. Then, N models are trained independently with a focal loss. The final prediction is the average of the predictions of the N models. We use a focal loss with the default $\gamma = 2$, and set the class weight α , to the inverse of the class ratio in each of the N bags.

$$\alpha = \frac{|Q|}{N|P| + |Q|} . \quad (14)$$

The optimal N is chosen via a validation set. Moreover, RiskMonitor suffers from a distribution shift between the training and evaluation sequences (NuScenes and NeuroNCAP, see Fig. D4). We alleviate this problem with Mixup (Zhang et al. 2017), which improves model generalization on OOD data (Thulasidasan et al. 2019).

5 Experiments

We first introduce RBD, GMM, and MCD baselines to which RiskMonitor is compared in Sec 5.1; and evaluation metrics in Sec. 5.2. We then evaluate RiskMonitor on real-world driving logs (Sec. 5.3) and in neural rendered closed-loop (Sec. 5.4). Finally, we ablate components and hyperparameters in Sec. 5.5; and distribution shifts between training and testing in Sec. D.3.

5.1 Collision Predictors

To the best of our knowledge, there is no existing work on collision risk estimation for end-to-end planners. We therefore compare to three prediction-driven baselines which map predictions to collision risk and one token-driven baseline (see Fig. 1).

Rule-based Discriminator(RBD): We compare the planning trajectory with the future locations of other road users and see if they will

intersect. Since the true future locations are not available, motion prediction is used as a proxy. We take the collision loss function in UniAD and VAD and feed their own planning waypoints, detected bounding boxes, and motion trajectories. With their own detected bounding boxes, the geometric dimensions of traffic road users are accounted for. **GMM:** In end-to-end planners, each road user’s multimodal trajectory, $\hat{\tau}_{\text{motion}}$, at each step is described as a GMM. Specifically, the trajectory of each road user consists of a set of possible future trajectories, each with corresponding probabilities. We use this set to define a sequence of chained GMMs. Collision risk is a combinatorial product of the collision probability in each GMM. See Sec. A.2 for details about these predictors.

Monte Carlo Dropout: MCD is a UQ technique that uses dropout during inference by performing multiple stochastic forward passes and obtaining an ensemble of predictions. We use the dropout in the last linear layer of the planning head (See Sec. A.1) to obtain an ensemble of planned trajectories $\{\hat{\tau}_{\text{plan}}^i\}$. The covariance of the endpoints of $\{\hat{\tau}_{\text{plan}}^i\}$ is calculated as an uncertainty score, which serves as a collision risk estimation.

LP-FCN: We adopt the model in previous loss prediction work (Kirchhof et al. 2024, 2023), a two-layer fully-connected network that maps the plan token to the loss value of an end-to-end planner. It is trained in the same settings as our RiskMonitor. As the plan token is obtained with BEV feature awareness, FCN has the potential to generalize. But it is not aware of the surrounding road users. This is to show that deep features from the last layer in traditional loss prediction work cannot directly transfer to complex end-to-end planners. Feature selection is further ablated in Sec. 5.5.

5.2 Evaluation Metrics

Since we treat CRE as a binary classification problem, we use area under the ROC curve (AUROC) and average precision (AP) to evaluate the performance of RiskMonitor. Since AP is known to be more sensitive to data imbalance, it is more suitable for real-world evaluation in Sec. 5.3. We also report precision at recall levels of 30%, 50%, and 70%, which indicate how many false positives (FP) we must accept to find a certain percentage of collisions. For the closed-loop evaluation,

the collision rate (Ljungbergh et al. 2024) is used to reflect RiskMonitor’s collision avoidance ability integrated with end-to-end planners.

5.3 Open-Loop Classification

Firstly, our RiskMonitor is evaluated on the real-world benchmark, nuScenes. UniAD and VAD are both trained and evaluated on the real-world dataset nuScenes. Note that nuScenes training and validation splits contain different sequences. We cache the h_{plan} , h_{motion} , and $L_{\text{collision}}$ of both planners on each split to build the training and test sets for RiskMonitor. A subset of the training set is held out as the validation set. In UniAD, various levels of safety distance are used for the collision loss, meaning $L_{\text{collision}} > 0$ if a road user’s distance to the ego-vehicle is within the safety distance. In RiskMonitor, we use $L_{\text{collision}}$ with 1 meter as the safety distance. There is no such setting in (Jiang et al. 2023), so we reimplement UniAD’s collision loss in VAD and use the same safety distance for both models. There are around 7.7% training samples and 8% test samples labeled as collision class for UniAD tokens. There are around 5.96% training samples (h_{plan} , h_{motion}) and 6.18% test samples labeled as collision class for VAD tokens. The bagging ensemble described in Sec. 4.3 is used in training to help alleviate this imbalance. See more details on the training in the Sec. B.

Results: Tab. 1 compares the performance of collision predictors based on prediction and tokens. For UniAD planner, RBD and GMM performances are barely above random guessing. A large number of false-positive predictions is the main reason for the low accuracy of RBD. The reasons for false-positive predictions include accumulated error in object detection, noisy ego-vehicle plan, and incorrect motion predictions. Fig. D3 visualizes examples of false-positive prediction from the rule-based discriminator based on UniAD prediction. Fig. D3 (a) and (b) show accumulated error from object detection. The front camera view shows that the ego-vehicle is driving straight forward, and there is no road user coming towards it. However, the BEV says that the road user (purple boxes) charges straight and collides head-on. Fig. D3 (d) shows wrong motion predictions. Front camera views indicate the white car on the left is driving in the same direction as the ego-vehicle; however, the corresponding blue boxes indicate

the opposite. Fig. D3 (e) shows a noisy ego plan. Front left camera views suggest the ego-vehicle is moving slowly, while the ego plan becomes noisy in BEV (red boxes).

The performance of the LP-FCN is significantly better than rule-based approaches and our proposed RiskMonitor gains the best performance. Pr50 suggests that to be able to find half of the collision samples, there are fewer than 70% FP predictions. For VAD, we see a similar performance. Though the VAD tokens are more imbalanced, RiskMonitor achieves surprisingly better performance. This indicates that the quality of tokens from the target model can affect RiskMonitor performance.

Planner	Method	AUROC	AP	Pr30	Pr50	Pr70	Pr100
UniAD	MC Dropout	50.0	7.9	8.1	7.6	7.8	8.1
	UniAD-RBD	54.24	12.75	9.58	7.26	7.26	7.26
	GMM	56.3	8.2	8.6	7.5	8.3	7.3
	LP-FCN	80.4	27.1	34.4	29.4	21.6	8.2
VAD	RiskMonitor	80.3	36.7	45.1	31.3	20.0	8.1
	VAD-RBD	60.3	8.4	8.8	8.1	6.7	6.7
	GMM	61.2	7.8	7.6	7.2	6.8	6.7
	LP-FCN	78.8	17.2	24.0	21.1	14.4	6.7
	RiskMonitor	92.2	43.2	48.1	45.6	39.5	6.9

Table 1: Classification performance comparison of different collision predictors on the open-loop benchmark nuScenes, for both UniAD and VAD. All the values are percentages, with higher being better.

5.4 Closed-loop Validation

We evaluate our RiskMonitor on NeuroNCAP (Ljungbergh et al. 2024), which is a closed-loop neural simulator containing safety-critical scenarios. We first test the closed-loop classification performance as in the open-loop case, then validate its collision-avoidance ability by thresholding on the risk.

5.4.1 Closed-loop classification

We use the same settings as in NeuroNCAP, where UniAD and VAD are only pretrained on nuScenes, to cache tokens in the end-to-end AD planners. We split them into training, validation, and test sets with a 6:1:3 ratio. The fraction of collision samples in the test set is 46% (see Sec. B for details). Each

set contains all three types of scenarios but strictly avoids using the same sequence in both sets to reduce the risk that the model learns the sequences rather than the task.

Results: The models are trained for 20 epochs with a learning rate set as 0.001, and the results are shown in Tab. 2. For training RiskMonitor and LP-FCN, we use focal loss with $\alpha = 0.5$ and $\gamma = 2$. The qualitative examples of RiskMonitor are shown in Fig. 2.

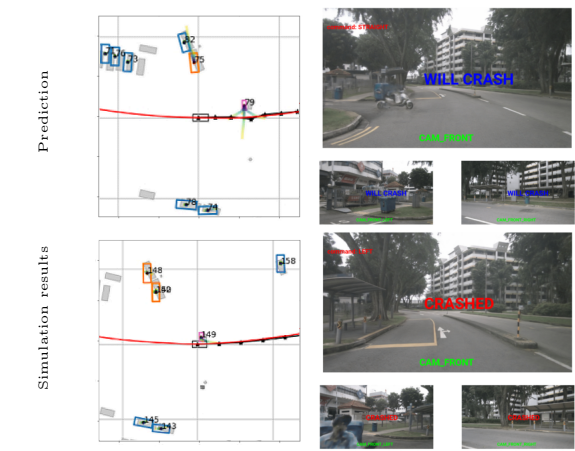
Model	AUROC	AP	Pr30	Pr50	Pr70	Pr100
MC Dropout	50.1	46.7	50.1	48.6	47.3	45.6
GMM	49.4	43.1	44.3	49.8	44.7	45.3
LP-FCN	64.7	56.5	56.0	56.4	58.8	45.8
RiskMonitor	70.6	66.7	77.2	67.5	59.4	45.8

Table 2: Classification performance comparison on the closed-loop benchmark, NeuroNCAP. All the values are percentages.

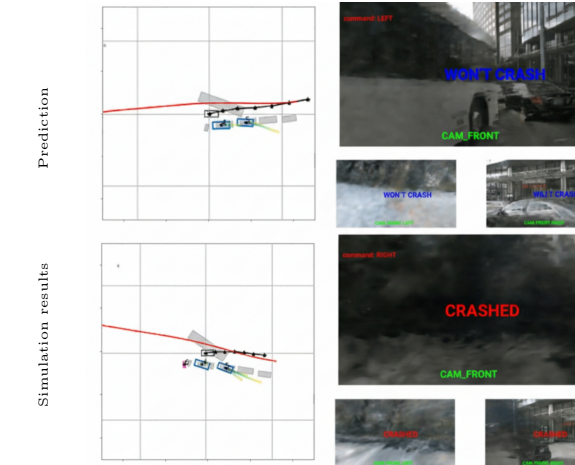
Analysis: The results presented in Tab. 2 demonstrate the effectiveness of RiskMonitor in identifying potential collisions across safety-critical scenarios. GMM achieves an AUROC of 49.4% and AP of 43.1%, indicating that its performance is close to random guessing. This suggests that it is not sufficient to estimate collision risk from an object-level interface. MC Dropout also performs close to a random guess. It shows that the standard UQ baseline fails in end-to-end planners trained with a large amount of losses.

By contrast, the LP-based model significantly improves detection performance, suggesting that learning a direct mapping from h_{plan} token to collision likelihood is beneficial. It is more efficient than MC Dropout, which requires several forward passes of the planners. RiskMonitor outperforms all baselines, achieving an AUROC of 70.6% and AP of 66.7%, indicating its better capability to capture collision-critical factors. This suggests that by cross-attending ego planning and road user dynamics, RiskMonitor improves collision detection for diverse simulated safety-critical scenarios.

Qualitative Results: We present qualitative results for true positive and false negative predictions in Fig. 2a and Fig. 2b, respectively. On the left of Fig. 2b, the BEV display reveals that the UniAD model fails to detect the bus (the



(a) Example of true positive prediction. Top: RiskMonitor predicts “will crash” at time t ; Bottom: Simulation result shows “crash” after a few steps.



(b) Example of false negative prediction. Top: RiskMonitor predicts “won’t crash” at time t ; Bottom: Simulation result shows “crash” after a few steps.

Fig. 2: Qualitative Examples on NeuroNCAP Simulation with UniAD as the end-to-end planner. The left figure presents ground-truth objects (gray) alongside predicted objects (color-coded by category) and their forecasted trajectories (blue-to-yellow gradient line) in BEV. It also depicts the ego-vehicle (black), the planned trajectory (black), and the reference trajectory (red), indicating its intended turn. The right figures are the inputs of the 3 front cameras. Best viewed in color.

huge grey rectangular without a blue box indicates the wrong detection result) in front of the ego vehicle. Consequently, the motion token lacks information about the bus, leading RiskMonitor to misclassify the scenario. This suggests that the accuracy of the perception modules in the AD model directly influences the predictive capability of RiskMonitor.

In contrast, in the True Positive (TP) example shown in Fig. 2a, UniAD provides more accurate coordinate estimations for a nearby object (indicated by the purple box), allowing RiskMonitor to correctly predict the collision. Interestingly, the plan from UniAD is still going straight even if there is a detected road user coming from the side. This highlights the necessity of having collision prediction when deploying end-to-end planners for AD. This further underscores the importance of reliable perception in downstream collision forecasting, as inaccuracies in detected objects or predicted motions can propagate errors into higher-level decision-making models.

5.4.2 Collision Avoidance

To further validate the impact of RiskMonitor, it is integrated with UniAD into NeuroNCAP pipeline to affect the control signal. The controller is adapted so that it slams on the brake with the maximum deceleration if the predicted collision risk is above a predetermined threshold. We keep the same settings and compare with baseline, and UniAD with or without test-time collision optimization in NeuroNCAP. The baseline in NeuroNCAP utilizes the perception outputs from UniAD: a braking maneuver is applied when objects detected in a corridor in front of the ego-vehicle. The collision rate is reported for three simulation scenarios.

Results: Tab. 3 shows that using our UniAD-RiskMonitor (U-R) significantly reduces collision rate for side and frontal sequences compared with the baseline while maintaining the rate on stationary scenes. As the baseline only considers road users running into a corridor in front of the ego-vehicle, it could ignore road users that are approaching from a side out of range. In frontal scenarios, road users coming towards a high speed could be detected too late and thus there is no sufficient time to brake for the baseline. RiskMonitor takes the road user motion tokens as the

	Scene	Base-U	UniAD	U-opt	Our U-R
Collision rate (%)	Stat	9.6	87.80	34.8	9.00
	Frontal	100.0	98.40	92.40	53.00
	Side	100.0	79.60	78.80	7.00
	Avg	69.90	88.60	68.70	23.00

Table 3: Closed-loop validation of RiskMonitor’s collision avoidance capability.

input, thus it can detect in a further range and brake in advance. UniAD, with or without post-processing, improves over the baseline but still reaches high collision rates. It shows that the planning module fails to adapt according to upstream detections. Through this experiment, the necessity of an auxiliary collision monitor is demonstrated.

5.5 Ablation

Next, we ablate the components of RiskMonitor and the hyperparameters. All the results are based on UniAD tokens on nuScenes and NeuroNCAP. All the ablation results are in terms of AP. The found optimal hyperparameters apply to the experiments in Sec. 5.3 and Sec. 5.4. See more ablations in Sec. C.

Feature selection and architectural assumptions: In Sec. 5.3 and Sec. 5.4, RiskMonitor is compared with LP-FCN with the plan token as the input. Here, we further explore the feature selection and architecture. Features from different UniAD task heads at different abstract levels on nuScenes are trained and tested separately as the sole input. For example, h_{BEV} is cached from the BEV encoder, and h_{track} and h_{traj} are from the tracking transformer and motion transformer. We use CNN to efficiently train on h_{BEV} , while h_{track} and h_{traj} are trained separately with self-attention RiskMonitor (See Sec. B.). In Tab. 4, none of them surpasses RiskMonitor’s performance trained on plan and motion tokens. It proves the validity of our chosen feature set and architecture.

6 Discussion and Limitations

Firstly, our RiskMonitor is efficient compared with ensemble-based uncertainty quantifiers; e.g., MC Dropout takes several forward passes of end-to-end planners. Though GMM and RBD only require one forward pass, they fail to capture

Features	BEV	Track	Motion	Plan+Motion
AP	32.57	30.51	31.42	36.7
AUROC	79.94	79.19	76.02	80.3

Table 4: Comparison of different choices of features and corresponding architecture design on nuScenes. The performance is reported on the test set of nuScenes tokens.

the inherent uncertainty in the plan. Second, both aleatoric and epistemic uncertainty can cause high collision loss values in end-to-end planners (Lahlou et al. 2021). Thus, we believe our RiskMonitor can be applied to OOD scenarios as long as its training tokens contain scenarios where the end-to-end planner is subject to OOD data.

We see two main limitations. First, we reveal that there is a distribution shift of different driving video sequences (see Sec. D.3). This is the main reason why the test performance drops on the test set compared to on the validation set in Sec. C. Second, despite NeuroNCAP being a SotA benchmark, it has several limitations, e.g., not being able to model adverse weather conditions, friction, suspension, or deformable objects.

7 Conclusion

Ensuring that self-driving vehicles do not cause road collisions is of paramount importance. We have presented RiskMonitor, which is an efficient and novel plug-and-play module for predicting collision risk using tokens from modern end-to-end AD models. RiskMonitor predicts whether the collision loss, which is commonly used to train end-to-end planners, is positive given the planned waypoints. This prediction corresponds nicely to a probability of a collision happening, allowing us to threshold it and reject decisions with high risk. In an ablation, we have demonstrated that tokens from the ego-vehicle planning and road user trajectory prediction modules of SotA end-to-end AD models are the most effective set. RiskMonitor outperforms common post-hoc rule-based approaches in both open-loop and closed-loop settings by avoiding accumulated prediction error in end-to-end planners. When integrated with a simple braking policy, RiskMonitor improves collision avoidance ability by 66.5% on average,

when tested closed-loop on safety-critical scenarios. Despite limitations, we are confident that our RiskMonitor approach to collision risk estimation is a major step towards safer AD vehicles.

Declarations

Conflict of interest statement The authors declare that they have no known competing financial interests or personal relationships that could have appeared to influence the work reported in this paper.

Funding Information This work was funded by Swedish national strategic research environment ELLIIT, grant C08. Computations for this work were enabled by the National Academic Infrastructure for Supercomputing in Sweden (NAIIS) and the Berzelius resource provided by National Supercomputing Centre at Linköping University and the Knut and Alice Wallenberg foundation, partially funded by the Swedish Research Council through grant agreement no. 2022-06725. This project is also supported by the Wallenberg AI, Autonomous Systems, and Software Program (WASP) funded by the Knut and Alice Wallenberg Foundation.

Data Availability This work does not propose any new dataset. The dataset (Caesar et al. 2020) that support the findings of this study is openly available at the URL: <https://www.nuscenes.org/>

Appendix A Details about Collision Predictors

A.1 Monte Carlo Dropout

Dropout Rate used during experiment is 0.1. It takes around 2 hours and 16 mins to do inference on nuScenes validation split for one epoch on single A100 GPU and at least 3 epochs to form the ensemble. Though MCD requires no additional caching or training process, it much more computational heavy compared to our RiskMonitor.

A.2 Gaussian Mixture Model

The End2End planner of most AD systems provides a motion prediction $\hat{\tau}_{\text{motion}} \in \mathbb{R}^{N_a \times N_m \times N_T \times 2}$ for each road user, in the form of an ensemble of N_m possible future trajectories with corresponding probabilities $\{\pi_m\}_1^M$, for each individual trajectory (Hu et al. 2023). We let these define a chain of GMMs, one for each time step k and road user a :

$$p(x_k|t_{a,k}) = \sum_{m=1}^{N_m} \pi_m \mathcal{N}(x_k - \hat{\tau}_{\text{motion}_{a,k,m}}, \Sigma_k) \quad (\text{A1})$$

The covariance Σ_k is set to be the size of ego-vehicle when $k = 1$, and linearly increasing with the prediction time, i.e. $\Sigma_k = k\sigma_0 \mathbf{I}$.

As in model-based collision avoidance literature (Zhou et al. 2023), we model the chance of crashing into a specific road user at a given time step as the integral over the area of the ego-vehicle bounding box, denoted by D .

$$P(\text{collision}|a, k) = \iint_D p(x_k|t_{a,k}) \quad (\text{A2})$$

The chance of crashing into at least one road user at a given time step is

$$P(\text{collision}|t_k) = 1 - \prod_{a=1}^{N_a} (1 - P(\text{collision}|a, k)) \quad (\text{A3})$$

The chance of getting at least one crash within the time horizon is

$$P(\text{collision}) = 1 - \prod_{t=1}^T (1 - P(\text{collision}|t_k)) \quad (\text{A4})$$

It also takes one inference forward process to evaluate. Though more efficient compared with RiskMonitor, the performance is limited.

Appendix B Experimental Details

B.1 Computing Environment for Experiments

All the experiments were run on a single Nvidia A100 GPU with the Linux operating system.

Python 3.8.10 and Pytorch 1.9.1 are used. It takes around 4 minutes to train one epoch and in total 20 epochs to converge.

B.2 Cache tokens

We use the pretrained checkpoints in the official GitHub repositories of UniAD and VAD during all the experiments. The caching process takes place during the last training epoch of the planner, which means that the test-time optimization in UniAD is not used. Due to this, there are more collision samples than the collision rate reported in (Hu et al. 2023). We cache the token after the attention module between the raw plan token and BEV features, before the final regression branch `self.reg_branch` that generates the final waypoints. See the code in the original repository: https://github.com/OpenDriveLab/UniAD/blob/v2.0/projects/mmdet3d_plugin/uniad/dense_heads/planning_head.py#L190

We cache the tokens as the input to the final regression branch `self.ego_fut_decoder`. See the code in the original repository: https://github.com/hustvl/VAD/blob/36047b6b5985e01832d8a2ecb0355d7f3c753ee1/projects/mmdet3d_plugin/VAD/VAD_head.py#L792

B.3 Training Details for Collision Predictors

nuScenes: Specifically, we use an ensemble of size 4 and $\alpha_f = 0.75$ in the focal loss, and the mixup parameter $\alpha_m = 3.0$. Both RiskMonitor and LP-FCN use the same batch size, optimizer, bagging ensemble, and focal loss.

B.4 A Balanced NeuroNCAP Dataset

AD models in NeuroNCAP are used for inference only, i.e., in the official GitHub repository there is no collision loss implementation since it only requires inference process in close-loop evaluation. Therefore, we transplant the collision training loss to the End2End AD models. To construct a balanced simulated dataset using NeuroNCAP, we first generate safety-critical scenarios using the NeuRAD simulator (Tonderski et al. 2024), which is capable of simulating three types of collision scenarios: *frontal*, *side*, and *stationary*. Each scenario

type consists of multiple scene-sequence pairs: five for frontal (0103, 0106, 0110, 0346, 0923), five for side (0103, 0108, 0110, 0278, 0921), and ten for stationary (0099, 0101, 0103, 0106, 0108, 0278, 0331, 0783, 0796, 0966).

For each scene-sequence pair, we initially conduct 100 simulation runs, recording the number of timestamps and the number of collision timestamps. This provides a preliminary statistical analysis of the dataset. Given these statistics, we assume that for any scene-sequence pair i , the number of timestamps per run (t_i) and the collision-to-timestamp ratio remain constant. That is, each run r_i of a particular scene-sequence pair produces c_i collisions and t_i timestamps.

To ensure a balanced dataset while maintaining a realistic overall collision rate, we formulate an Integer Linear Programming (ILP) problem. The objective is to minimize the largest difference D in the number of runs among all scene-sequence pairs:

$$\min_{r_i} D \quad (B5)$$

subject to the following constraints:

$$|r_i - r_j| \leq D, \quad \forall i, j \quad (B6)$$

$$r_i \geq 45, \quad \forall i \quad (B7)$$

$$\sum_i c_i \cdot r_i \geq 0.46 \sum_i t_i \cdot r_i \quad (B8)$$

$$\sum_i c_i \cdot r_i \leq 0.54 \sum_i t_i \cdot r_i \quad (B9)$$

$$\sum_i r_i \leq 1200 \quad (B10)$$

These constraints ensure that: (1) the variation in the number of runs among scene-sequence pairs is minimized, (2) every scene-sequence pair is used at least 45 times to maintain diversity, (3) the total collision rate remains within 49%–51%, and (4) the total number of runs does not exceed 1200. Solving the ILP in Eq. B5 yields the optimal number of runs r_i for each scene-sequence pair.

Once the optimal values of r_i are determined, we execute the corresponding simulation runs in NeuroNCAP, generating a well-balanced dataset that effectively captures safety-critical driving scenarios. This dataset serves as the foundation for evaluating the performance of RiskMonitor and

other models in diverse and challenging collision scenarios.

Appendix C Additional Ablations

C.1 Bagging and Focal loss

Here we report the effect of different numbers of bagging ensembles and the corresponding focal loss. In NeuroNCAP, we can balance the classes (see Sec. B.4), and thus the result is reported only on nuScenes in Tab. C1. We can see that having bagging ensembles of size four gives the best performance on both sets and alleviates the class imbalance issues between collisions and non-collisions in nuScenes.

Ensemble splits	1	2	3	4	6	12
Col:No-Col	1:12	1:6	1:4	1:3	1:2	1:1
α : Ratio	12/13	6/7	4/5	3/4	2/3	1/2
Val AP	63.5	64.4	65.3	66.6	63.9	63.5
Test AP	26.0	26.8	26.9	32.3	31.0	28.2

Table C1: Ablation on Bagging Ensemble size and α_f in Focal Loss. No mixup is used during training.

C.2 Mixup

Here we report the effect of mixup (Zhang et al. 2017) on top of the bagging ensemble. There is one hyperparameter α_m that governs the strengths of interpolation between sample-target pairs. On nuScenes in Tab. C2b, as α_m increases, AP keeps improving until the value reaches 3.0. This value is higher than the default value $\alpha_m = 1.0$. The corresponding Beta function is unimodal, which means there is a higher chance of having a mixup coefficient λ close to 0.5 than the default value. On NeuroNCAP in Tab. C2a, there is a similar trend, whereas the optimal AP is achieved at $\alpha_m = 1.0$. More spread training tokens (visualized in Fig. D4b) could explain the difference.

C.3 Transformer decoder layers

We also study the effect of having more layers of transformer decoder. We use the default value $\alpha_m = 1.0$ for the Beta distribution in the mixup.

α_m	0.1	0.2	0.3	0.4	0.5	0.6	0.7
Val	62.5	61.0	64.1	66.4	63.1	63.2	62.8
Test	59.6	62.1	62.1	65.9	63.6	62.4	60.8
α_m	0.8	0.9	1.0	2.0	3.0	4.0	6.0
Val	63.8	65.3	66.5	66.0	66.2	66.0	64.8
Test	62.2	64.3	66.7	66.3	66.1	66.7	64.4

(a) NeuroNCAP

α_m	0.1	0.2	0.3	0.4	0.5	0.6	0.7
Val	64.7	64.5	64.7	64.8	64.9	64.8	64.8
Test	30.7	32.3	33.4	33.3	33.1	32.8	31.6
α_m	0.8	0.9	1.0	2.0	3.0	4.0	6.0
Val	66.1	63.5	67.7	66.8	65.6	65.2	63.2
Test	34.5	33.0	35.6	34.7	36.7	35.0	36.4

(b) nuScenes

Table C2: Ablation on α_m for Mixup.

The result is in Tab. C3. Surprisingly, adding more transformer decoder layers leads to a performance decrease on both nuScenes and NeuroNCAP. We speculate that this could be due to the distribution shift, as shown in Sec. D.3, and that using more transformer layers risks overfitting the training set.

# layers	Mixup			No Mixup		
	1	2	3	1	2	3
Test	66.7	63.6	65.6	64.3	59.2	64.1

(a) NeuroNCAP

# layers	Mixup			No Mixup		
	1	2	3	1	2	3
Val	67.4	65.9	62.2	66.6	64.2	61.0
Test	35.6	33.0	31.2	32.3	31.4	26.3

(b) nuScenes

Table C3: Comparison of decoder layer effects with and without Mixup.

Appendix D Additional Results

D.1 Baseline Results

See Fig. D3 for FP predictions from RBD baseline.

D.2 Qualitative Examples on NeuroNCAP Dataset

We demonstrate qualitative examples in the NeuroNCAP Simulation Dataset with UniAD as the

end-to-end planner. The true positive examples in which RiskMonitor has succeeded in predicting collisions are shown in Fig. D1, while false negative examples in which RiskMonitor fails to predict collisions are shown in Fig. D2.

As seen in the first and third images of Fig. D2, the AD model’s predicted coordinates for objects near the ego-vehicle are inaccurate. In the first image, for example, the ground truth distance to the ego-vehicle is farther than the estimated distance. In the third image, the failure to detect the object ahead results in incorrectly classifying a collision sample as a non-collision. Additionally, in the second sample, our model’s incorrect prediction may have been caused by the AD model’s erroneous estimation, where a stationary object was misunderstood as moving by motion token.

In the true positive examples shown in Fig. D1, UniAD provides more accurate coordinate estimations for a nearby object, allowing RiskMonitor to accurately identify the collision.

D.3 Distribution Shift Analysis

In Sec. D and Sec. C, we note that the performance on the validation tokens is substantially better than on the test tokens. During experiments in Sec. 5.4, we also note that the test performance is nearly perfect if we allow training tokens and test tokens from the same sequence, even if they belong to different scenario types. This indicates that it is the distribution shift between different AD video sequences that hinders RiskMonitor from generalizing and thus causes a drop in the performance on test tokens.

In Fig. D4, we use the t-SNE algorithm to reduce the dimension of plan tokens and visualize them in 2D space. we visualize the planning token h_{plan} from UniAD on nuScenes in both the training and validation split. In Fig. D4a, it is notable that (1) there are two clusters at the top, mixed with training and test samples, and one larger cluster at the bottom, mainly consisting of training samples; (2) there is a hole in the bottom cluster, which happens to be filled with test samples that are FP predictions; (3) there are more TP predictions in the top two clusters, where there seem to be less distribution shift between training and test samples. In Sec. D, we further visualize the corresponding video sequence of these samples and find that

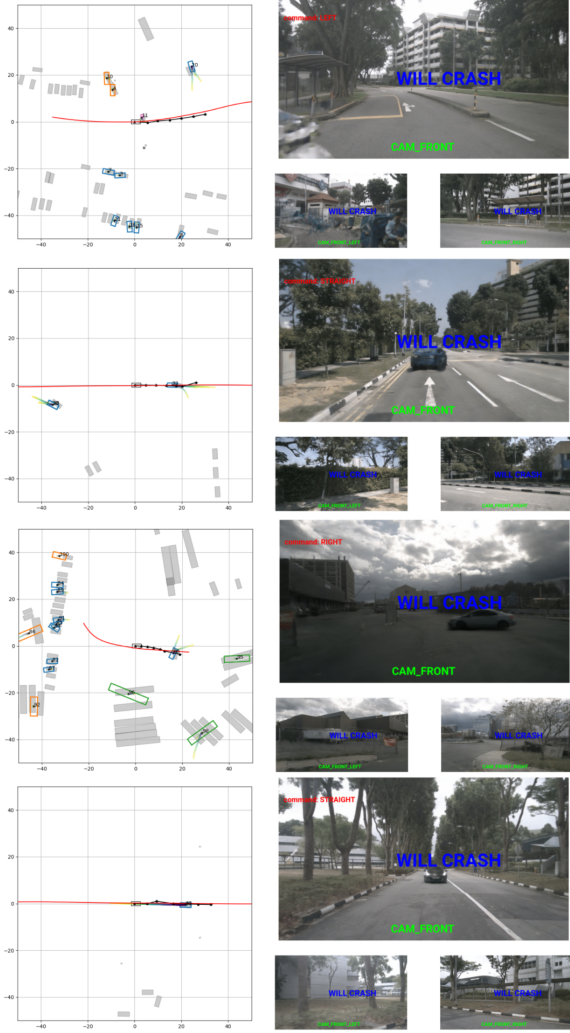


Fig. D1: True Positive Examples on NeuroNCAP Simulation Dataset (Scenarios from top to bottom: side, stationary, stationary, frontal)

the top-left cluster roughly corresponds to turning right in the video, the top-right cluster roughly corresponds to turning left, and the bottom cluster roughly corresponds to going straight. These findings reveal that the distribution shift between the plan and road user tokens that correspond to different sequences is significant. The distribution shift between nuScenes train and validation splits is the main reason for the performance drop of RiskMonitor on the test tokens. In mixup, setting $\beta = 3.0$ improves generalization since a convex combination of sample-target pairs has the potential to alleviate the gap.

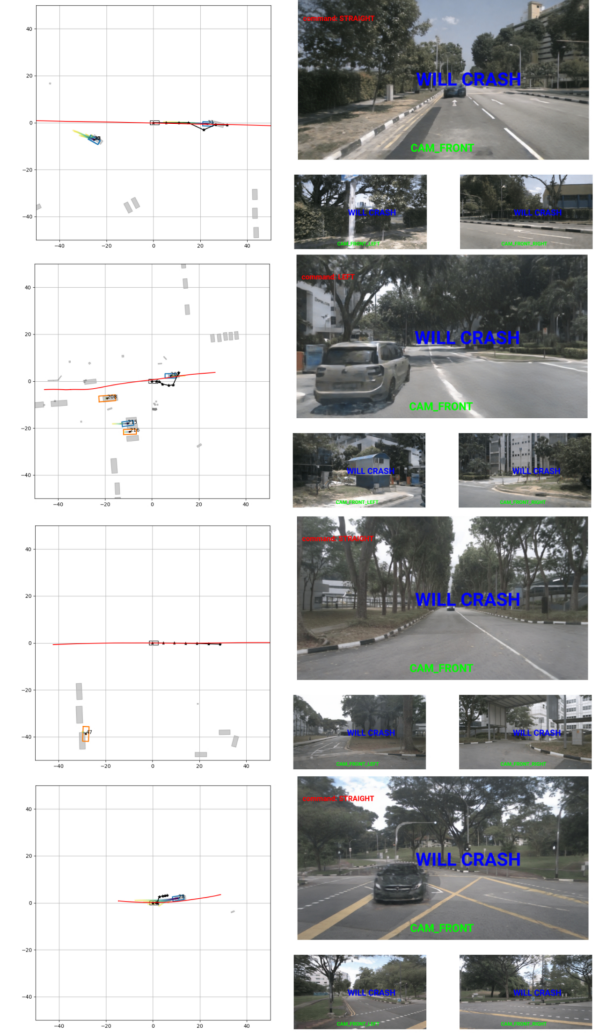


Fig. D2: False Negative Examples on the NeuroNCAP Simulation Dataset (Scenarios from top to bottom: stationary, stationary, frontal, frontal)

In Fig. D4b, we similarly visualize the plan tokens h_{plan} on NeuroNCAP, which also exhibit distinct clusters corresponding to different scenario types and sequences. The distribution appears more dispersed than in nuScenes, reflecting the greater variability and discreteness introduced by the simulation environments. In addition, the overlap between training and test samples is relatively low, indicating a significant distribution shift between the test and training sets with different scenarios and sequences. These distribution shifts become more pronounced when a particular scenario type or sequence has little

resemblance to the training distribution. Consequently, RiskMonitor’s performance declines for tokens lying far from learned regions of the feature space.

D.4 Scenario Cases Corresponding to Different Clustering

Fig. [D5](#) visualizes the three front views in the training sequences from different clusters in Fig. 3a in the main paper. Each cluster corresponds to turning left, turning right and going straight plan.

D.5 Visualization Plot of the Quantity Result

Precision-Recall and ROC curves for Tab. 2 of UniAD and VAD on nuScenes validation split are shown in Fig. [D6](#).

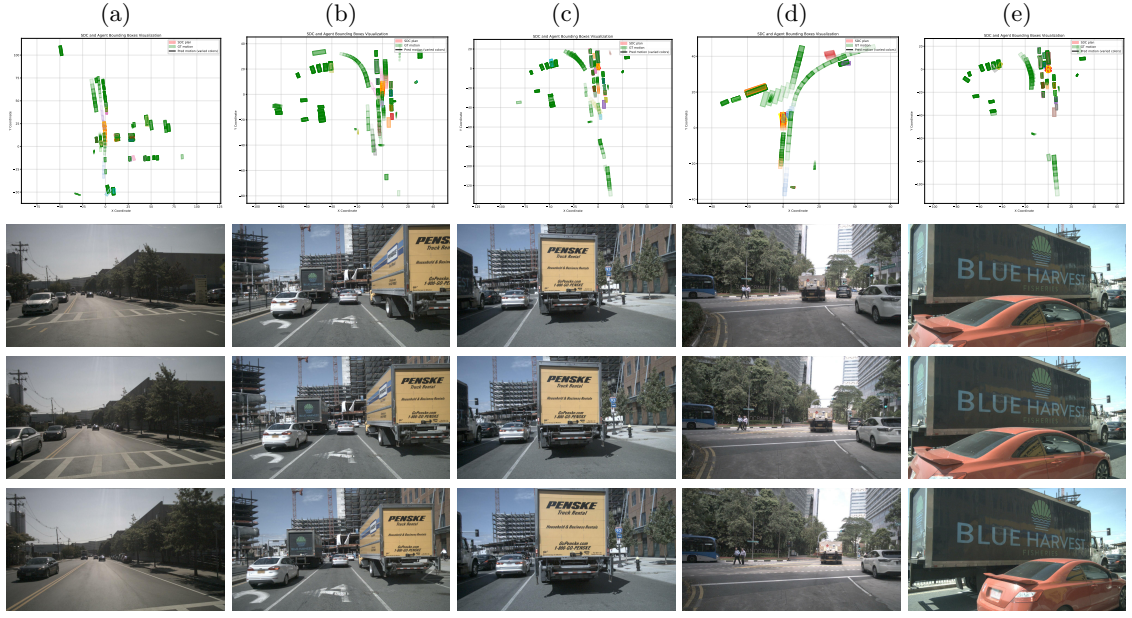


Fig. D3: Visualization of FP predictions from rule-based discriminator on nuScenes. Row 1 shows BEV bounding box visualizations, and increasing intensity of a color indicates the future steps. Row 2-4 show corresponding CAM_FRONT or CAM_FRONT_LEFT camera images. Better review in color.



Fig. D4: 2D t-SNE plots for plan tokens h_{plan} from UniAD on nuScenes and NeuroNCAP. It is better to review in color. For the training tokens, we assign a color to distinguish collision and non-collision samples. For the test tokens, we assign colors based on the test results, true positives (TP), false positives (FP), true negatives (TN), and false negatives (FN).



(a) Cluster 0 (turn right)

(b) Cluster 1 (turn left)

(c) Cluster 2 (go straight)

Fig. D5: Front views of different clusters in Fig. D4. From top to bottom, images correspond to increasing time steps.

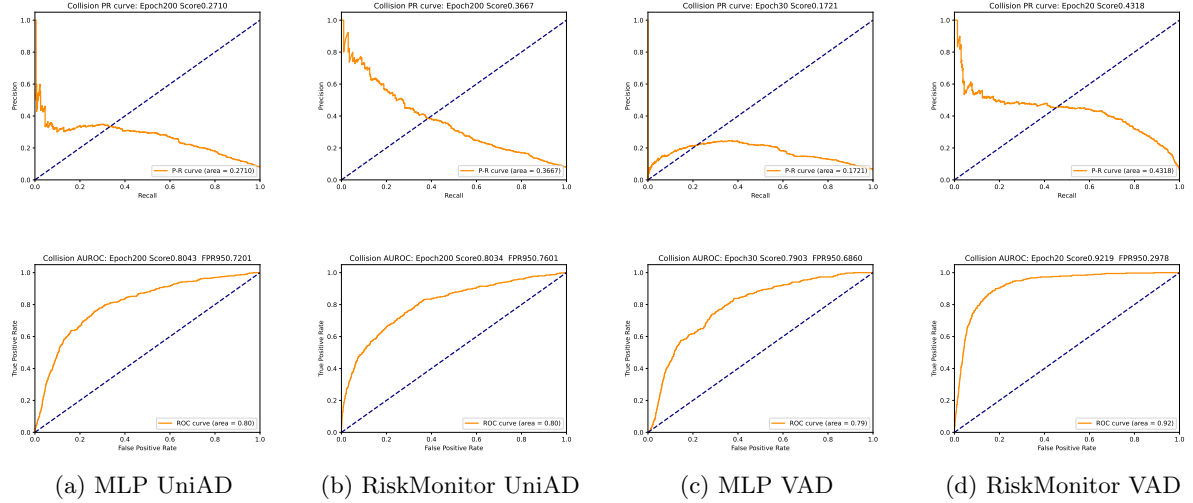


Fig. D6: Precision-Recall and ROC curves for nuScenes in the main paper.

References

Akan, A.K., Güney, F.: Stretchbev: Stretching future instance prediction spatially and temporally. In: European Conference on Computer Vision, pp. 444–460 (2022). Springer

Altendorfer, R., Wilkmann, C.: What is the collision probability and how to compute it (2017) <https://doi.org/10.48550/arXiv.1711.07060>

Bahari, M., Saadatnejad, S., Rahimi, A., Shaverdikondori, M., Shahidzadeh, A.-H., Moosavi-Dezfooli, S.-M., Alahi, A.: Vehicle trajectory prediction works, but not everywhere. arXiv. Version Number: 2 (2021). <https://doi.org/10.48550/ARXIV.2112.03909> . <https://arxiv.org/abs/2112.03909> Accessed 2025-07-04

Caesar, H., Bankiti, V., Lang, A.H., Vora, S., Lioung, V.E., Xu, Q., Krishnan, A., Pan, Y., Baldan, G., Beijbom, O.: nuscenes: A multimodal dataset for autonomous driving. In: Proceedings of the IEEE/CVF Conference on Computer Vision and Pattern Recognition, pp. 11621–11631 (2020)

Chen, D., Koltun, V., Krähenbühl, P.: Learning to drive from a world on rails. In: Proceedings of the IEEE/CVF International Conference on Computer Vision, pp. 15590–15599 (2021)

Codevilla, F., Müller, M., López, A., Koltun, V., Dosovitskiy, A.: End-to-end driving via conditional imitation learning. In: 2018 IEEE International Conference on Robotics and Automation (ICRA), pp. 4693–4700 (2018). IEEE

Cai, P., Wang, S., Sun, Y., Liu, M.: Probabilistic end-to-end vehicle navigation in complex dynamic environments with multimodal sensor fusion. IEEE Robotics and Automation Letters **5**(3), 4218–4224 (2020)

Chen, Z., Ye, M., Xu, S., Cao, T., Chen, Q.: Ppad: Iterative interactions of prediction and planning for end-to-end autonomous driving. In: Proceedings of the European Conference on Computer Vision (ECCV) (2024)

Dosovitskiy, A., Ros, G., Codevilla, F., Lopez, A.,

Koltun, V.: Carla: An open urban driving simulator. In: Conference on Robot Learning, pp. 1–16 (2017). PMLR

Deo, N., Wolff, E., Beijbom, O.: Multimodal trajectory prediction conditioned on lane-graph traversals. In: Conference on Robot Learning, pp. 203–212 (2022). PMLR

Gal, Y., Ghahramani, Z.: Dropout as a bayesian approximation: Representing model uncertainty in deep learning. In: International Conference on Machine Learning, pp. 1050–1059 (2016). PMLR

Houenou, A., Bonnifait, P., Cherfaoui, V.: Risk assessment for collision avoidance systems. 2014 17th IEEE International Conference on Intelligent Transportation Systems, ITSC 2014 (2014) <https://doi.org/10.1109/ITSC.2014.6957721>

Hu, S., Chen, L., Wu, P., Li, H., Yan, J., Tao, D.: St-p3: End-to-end vision-based autonomous driving via spatial-temporal feature learning. In: European Conference on Computer Vision, pp. 533–549 (2022). Springer

Hu, P., Huang, A., Dolan, J., Held, D., Ramanan, D.: Safe local motion planning with self-supervised freespace forecasting. In: Proceedings of the IEEE/CVF Conference on Computer Vision and Pattern Recognition, pp. 12732–12741 (2021)

Huang, C., Hang, P., Hu, Z., Lv, C.: Collision-probability-aware human-machine cooperative planning for safe automated driving. IEEE Transactions on Vehicular Technology **70**(10), 9752–9763 (2021) <https://doi.org/10.1109/TVT.2021.3102251>

Hu, A., Murez, Z., Mohan, N., Dudas, S., Hawke, J., Badrinarayanan, V., Cipolla, R., Kendall, A.: Fiery: Future instance prediction in bird’s-eye view from surround monocular cameras. In: Proceedings of the IEEE/CVF International Conference on Computer Vision, pp. 15273–15282 (2021)

Hu, Y., Yang, J., Chen, L., Li, K., Sima, C., Zhu, X., Chai, S., Du, S., Lin, T., Wang, W., *et al.*: Planning-oriented autonomous driving. In:

Proceedings of the IEEE/CVF Conference on Computer Vision and Pattern Recognition, pp. 17853–17862 (2023)

Hu, Y., Zhan, W., Tomizuka, M.: Probabilistic prediction of vehicle semantic intention and motion. In: IEEE Intelligent Vehicles Symposium (IV), pp. 307–313 (2018)

Jiang, B., Chen, S., Xu, Q., Liao, B., Chen, J., Zhou, H., Zhang, Q., Liu, W., Huang, C., Wang, X.: Vad: Vectorized scene representation for efficient autonomous driving. In: Proceedings of the IEEE/CVF International Conference on Computer Vision, pp. 8340–8350 (2023)

Jia, X., Yang, Z., Li, Q., Zhang, Z., Yan, J.: Bench2drive: Towards multi-ability benchmarking of closed-loop end-to-end autonomous driving. *Advances in Neural Information Processing Systems* **37**, 819–844 (2024)

Kirchhof, M., Collier, M., Oh, S.J., Kasneci, E.: Pretrained visual uncertainties. arXiv preprint arXiv:2402.16569 (2024)

Khurana, T., Hu, P., Dave, A., Ziglar, J., Held, D., Ramanan, D.: Differentiable raycasting for self-supervised occupancy forecasting. In: European Conference on Computer Vision, pp. 353–369 (2022). Springer

Kirchhof, M., Mucsányi, B., Oh, S.J., Kasneci, D.E.: URL: A representation learning benchmark for transferable uncertainty estimates. *Advances in Neural Information Processing Systems* **36**, 13956–13980 (2023)

Koopman, P., Wagner, M.: Challenges in autonomous vehicle testing and validation. *SAE International Journal of Transportation Safety* **4**(1), 15–24 (2016)

Lin, T.-Y., Goyal, P., Girshick, R., He, K., Dollár, P.: Focal loss for dense object detection. In: Proceedings of the IEEE International Conference on Computer Vision, pp. 2980–2988 (2017)

Lambert, A., Gruyer, D., Saint Pierre, G.: A fast monte carlo algorithm for collision probability estimation, pp. 406–411 (2009). <https://doi.org/10.1109/ICARCV.2008.4795553>

Lahlou, S., Jain, M., Nekoei, H., Butoi, V.I., Bertin, P., Rector-Brooks, J., Korablyov, M., Bengio, Y.: Deup: Direct epistemic uncertainty prediction. arXiv preprint arXiv:2102.08501 (2021)

Ljungbergh, W., Tonderski, A., Johnander, J., Caesar, H., Åström, K., Felsberg, M., Petersson, C.: NeuroNCAP: Photorealistic closed-loop safety testing for autonomous driving. In: European Conference on Computer Vision, pp. 161–177 (2024). Springer

Li, Z., Wang, W., Li, H., Xie, E., Sima, C., Lu, T., Yu, Q., Dai, J.: BEVFormer: Learning Bird's-Eye-View Representation from Multi-Camera Images via Spatiotemporal Transformers (2022). <https://arxiv.org/abs/2203.17270>

Malinin, A., Band, N., Ganshin, Alexander, Chesnokov, G., Gal, Y., Gales, M.J.F., Noskov, A., Ploskonosov, A., Prokhorenkova, L., Provilkov, I., Raina, V., Raina, V., Roginskiy, Denis, Shmatova, M., Tigas, P., Yangel, B.: Shifts: A Dataset of Real Distributional Shift Across Multiple Large-Scale Tasks. arXiv. Version Number: 3 (2021). <https://doi.org/10.48550/ARXIV.2107.07455> . <https://arxiv.org/abs/2107.07455> Accessed 2025-07-04

Meinhardt, T., Kirillov, A., Leal-Taixe, L., Feichtenhofer, C.: Trackformer: Multi-object tracking with transformers. In: Proceedings of the IEEE/CVF Conference on Computer Vision and Pattern Recognition, pp. 8844–8854 (2022)

Neumeier, M., Dorn, S., Botsch, M., Utschick, W.: Reliable trajectory prediction and uncertainty quantification with conditioned diffusion models, pp. 3461–3470 (2024). <https://doi.org/10.1109/CVPRW63382.2024.00350>

Nordlund, P.-J., Gustafsson, F.: Probabilistic Conflict Detection for Piecewise Straight Paths. Submitted to *Automatica* (2008)

Prakash, A., Chitta, K., Geiger, A.: Multi-modal fusion transformer for end-to-end autonomous driving. In: Proceedings of the IEEE/CVF Conference on Computer Vision and Pattern Recognition, pp. 7077–7087 (2021)

Philipp, A., Goehring, D.: Analytic collision risk calculation for autonomous vehicle navigation. In: 2019 International Conference on Robotics and Automation (ICRA), pp. 1744–1750 (2019). IEEE

Toit, N., Burdick, J.: Probabilistic collision checking with chance constraints. *Robotics, IEEE Transactions on* **27**, 809–815 (2011) <https://doi.org/10.1109/TRO.2011.2116190>

Thulasidasan, S., Chennupati, G., Bilmes, J.A., Bhattacharya, T., Michalak, S.: On mixup training: Improved calibration and predictive uncertainty for deep neural networks. *Advances in neural information processing systems* **32** (2019)

Tonderski, A., Lindström, C., Hess, G., Ljungbergh, W., Svensson, L., Petersson, C.: Neurad: Neural rendering for autonomous driving. In: Proceedings of the IEEE/CVF Conference on Computer Vision and Pattern Recognition, pp. 14895–14904 (2024)

Vaswani, A., Shazeer, N., Parmar, N., Uszkoreit, J., Jones, L., Gomez, A.N., Kaiser, Polosukhin, I.: Attention is all you need. In: NIPS'17: Proceedings of the 31st International Conference on Neural Information Processing Systems, pp. 6000–6010 (2017)

Wu, P., Chen, L., Li, H., Jia, X., Yan, J., Qiao, Y.: Policy pre-training for autonomous driving via self-supervised geometric modeling. In: 11th International Conference on Learning Representations, ICLR 2023 (2023)

Westny, T., Frisk, E., Olofsson, B.: Vehicle behavior prediction and generalization using imbalanced learning techniques. In: 2021 IEEE International Intelligent Transportation Systems Conference (ITSC), pp. 2003–2010 (2021). IEEE

Wiederer, J., Schmidt, J., Kressel, U., Dietmayer, K., Belagiannis, V.: Joint out-of-distribution detection and uncertainty estimation for trajectory prediction. In: 2023 IEEE/RSJ International Conference on Intelligent Robots and Systems (IROS), pp. 5487–5494 (2023). IEEE

Wang, S., Zhou, Q., Wu, K., Wu, D., Lee, W.-B., Wang, J.: Redoubt: Duo safety validation for autonomous vehicle motion planning. In: The Thirty-ninth Annual Conference on Neural Information Processing Systems (2025)

Yu, X., Franchi, G., Gu, J., Aldea, E.: Discretization-induced dirichlet posterior for robust uncertainty quantification on regression. In: Proceedings of the AAAI Conference on Artificial Intelligence, vol. 38, pp. 6835–6843 (2024)

Yoo, D., Kweon, I.S.: Learning loss for active learning. In: Proceedings of the IEEE/CVF Conference on Computer Vision and Pattern Recognition, pp. 93–102 (2019)

Yang, X., Zhang, G., Gao, F., Huang, H.: Risk-aware defensive motion planning for distributed connected autonomous vehicles. In: 2024 IEEE Transportation Electrification Conference and Expo (ITEC), pp. 1–6 (2024). <https://doi.org/10.1109/ITEC60657.2024.10598864>

Zhang, H., Cisse, M., Dauphin, Y.N., Lopez-Paz, D.: mixup: Beyond empirical risk minimization. arXiv preprint arXiv:1710.09412 (2017)

Zhou, J., Olofsson, B., Frisk, E.: Interaction-aware motion planning for autonomous vehicles with multi-modal obstacle uncertainties using model predictive control. *IEEE Transactions on Intelligent Vehicles* **9**(1) (2023)

Zheng, W., Song, R., Guo, X., Zhang, C., Chen, L.: Genad: Generative end-to-end autonomous driving. In: European Conference on Computer Vision, pp. 87–104 (2024). Springer